A theoretical study on the mechanism of the base-promoted decomposition of *N*-chloro,*N*-methylethanolamine†

Daniel R. Ramos,[a] Raquel Castillo,[b] Moisés Canle L.,[a] M. Victoria García,[a] Juan Andrés[b] and J. Arturo Santaballa*[a]

Received 10th November 2008, Accepted 9th February 2009
First published as an Advance Article on the web 2nd March 2009
DOI: 10.1039/b820006h

The first step of the base-promoted decomposition of *N*-chloro,*N*-methylethanolamine in aqueous solution ($CH_3N(Cl)CH_2CH_2OH + HO^- \rightarrow$ imine + Cl^- + H_2O (+ CH_2O) $\rightarrow$ amine + aldehyde) is investigated at the MP2/6-31++G(d,p) computing level. Solvation is included by using both a microsolvated model, in which two explicit water molecules simulate the specific solvent effects, and a hybrid cluster-continuum model, by applying a polarized continuum on the previous results, to account for the bulk effect of the solvent. Four alternative pathways (bimolecular fragmentation, Hofmann, Zaitsev and intramolecular eliminations) are possible for the rate-limiting step of this base-promoted decomposition. These reactive processes are bimolecular asynchronous concerted reactions. The common feature of the four pathways is the proton transfer to HO^- being more advanced than all other molecular events, whereas imine formation is delayed. Non-reactive cyclic arrangements involving one of the explicit water molecules are found at transition structures of Hofmann and Zaitsev eliminations, such water molecule acting both as H^+ donor and acceptor. Although MP2 calculations misjudge the absolute activation Gibbs free energy values, this computational level adequately predicts the enhancement in the decomposition rate due to the presence of the -OH group.

Introduction

Experimental and computational research devoted to the determination of reaction mechanisms is an issue of major concern in chemistry.[1] Theoretical characterization of geometry and energy of stationary points on potential energy surfaces (PESs) has significantly improved our understanding of intrinsic reactivity, helping to unravel the molecular mechanism of chemical reactions. However, molecular modelling of chemical processes in solution is a very demanding task; in this sense one of the currently accepted solvation models is to combine explicit water molecules, to mimic specific solute–solvent interactions at the first solvation shell, and a dielectric continuum to model bulk solvent properties.

Chemical reactivity involving *N*-halo compounds has been widely studied at a macroscopic level over the past 40 years due to their relevance to both environmental and biological chemistry.[2] In this sense, chlorination is still the most used method of water treatment,[3] despite its presumed relationship with cancer.[4] This fact together with the inability of aqueous chlorine to inactivate certain microorganisms have promoted the search of safer alternative water treatment methods, jointly known as advanced oxidation processes.[5] On the other hand, chlorination is essential in leukocyte protection against infection in mammals,[6–8] and it has also been related to cell lysis[7] and other disorders related to inflammation.[9] When leukocytes are activated, the enzyme myeloperoxidase reacts with chloride ion and hydrogen peroxide to generate either HOCl or an oxidizing enzyme complex, which chlorinate a wide variety of nitrogenated compounds.[10–12]

Formation and decomposition of numerous halogenated nitrogen species has been examined experimentally.[2] Chlorination of amines and amino acids by HOCl shows a complex dependence on acidity, its maximum rate appearing near neutral pH. After its formation, *N*-chloro compounds decompose; the higher the basicity of the medium, the faster their decomposition rate. Base-promoted decomposition of *N*-chloro derivatives of aliphatic secondary amines in aqueous solution is not particularly fast; for example, the corresponding second-order rate constant for the HO^--promoted decomposition of $CH_3N(Cl)CH_2CH_3$ is *ca.* 2×10^{-4} mol dm^{-3} s^{-1} at 298 K. The currently accepted mechanism for the base-promoted decomposition of *N*-chloro amines involves two consecutive steps. The first one is the rate-determining step of the reaction and corresponds with an elimination reaction, Hofmann or Zaitsev (see Scheme 1). The second step is the fast hydrolysis of the so-formed imine. Noticeable rate enhancement is observed when parent *N*-chloroethanolamines are considered;[13,14] for example the observed second order rate constant for the HO^--promoted decomposition of $CH_3N(Cl)CH_2CH_2OH$ is 360-fold higher than that of *N*-chloro,*N*-methylethylamine.[14] Such a rate increase could be ascribed to the inductive effect due to the -OH group, which should make more acidic the hydrogen being transferred, but product analysis did not support such a hypothesis. Unexpected production of formaldehyde was observed in the case of *N*-chloro,*N*-methylethanolamine, which was contrary to such

[a]*Chemical Reactivity & Photoreactivity Group, Dept. of Physical Chemistry & Chemical Eng. I, University of A Coruña, Alejandro de la Sota 1, E-15008, A Coruña, Spain. E-mail: danielr@udc.es, mcanle@udc.es, vicky@udc.es, arturo@udc.es; Fax: +34 981 167065; Tel: +34 981 167000*
[b]*Departament de Química Física y Analítica, Universitat Jaume I, Box 224, E-12080, Castelló, Spain. E-mail: rcastill@qfa.uji.es, andres@qfa.uji.es; Fax: +34 964 728066; Tel: +34 964 728067*

† Electronic supplementary information (ESI) available: Optimized molecular geometries in Cartesian coordinates, selected parameters and gas phase computed total energies in hartrees. See DOI: 10.1039/b820006h

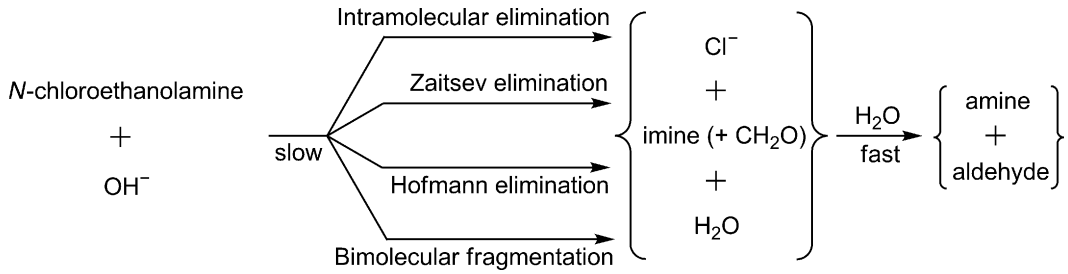

Scheme 1 General mechanism for the base-promoted decomposition of aliphatic secondary *N*-chloroethanolamines in aqueous solution.

an inductive effect; furthermore, non-stoichiometric amounts were found.

These facts are in agreement with two additional competitive pathways for the rate-determining base-promoted decomposition of secondary *N*-chloroethanolamines: bimolecular fragmentation and intramolecular elimination, which are responsible for the reaction rate enhancement (Scheme 1). Experimental data point to all four pathways being asynchronous concerted processes.[14]

Aminoalcohols are widely used as feedstock in the production of chemical intermediates, pharmaceuticals, polishes, detergents and emulsifiers. They have also relevant applications as corrosion inhibitors or for scrubbing certain acidic gases.[15] In particular, *N*-methylethanolamine is involved in the biosynthesis of choline, a precursor of acetylcholine in mammals, a neurotransmitter of the peripheral and the central nervous system.[16] It has also been proposed to play a role in the prebiotic synthesis of vitamin B6-type systems.[17] These compounds have beneficial therapeutic effect on cardiac diseases, such as cardiac fibrosis,[18] and might play a role in the regulation of synaptic vesicle filling.[19] *N*-Methylethanolamine is the simplest choice of the family, and thus was selected as model compound for the electronic structure calculation of the mechanism of decomposition of secondary *N*-haloethanolamines in alkaline medium. Hofmann elimination has been recently analyzed computationally by B3LYP using the 6-31++G(d,p) basis set,[20] and the description of the detailed mechanism is consistent with the experimental data.[14]

In this work, we present electronic structure calculations to shed light on the four parallel reaction pathways associated to the base-promoted decomposition of secondary *N*-haloethanolamines: Hofmann, Zaitsev and intramolecular eliminations, and bimolecular fragmentation (see Scheme 1). The model that revealed to be more appropriate[20] is used here at a higher computational level to examine the reaction between *N*-chloro,*N*-methylethanolamine and hydroxide ion. To model solvent effects, we have included two explicit water molecules simulating specific solute–solvent interactions, and further utilized the continuum method to take into account the effect of bulk solvent. The results are compared with previously obtained experimental data.[14]

Computational methods

All calculations have been carried out with the Gaussian98 suite of programs.[21] Minima and transition structures were fully optimized at the MP2 =full/6-31++G(d,p) computational level; the perturbation theory of Møller–Plesset truncated at the second order was used to consider the correlation energy.[22] The nature of the molecular mechanisms has been elucidated by characterizing stationary points on the PES: reactants (R), bound reactant-like complexes (called hereafter reactant interaction complexes (RIC)), transition structures (TS), and product interaction complexes (PIC), which open the channel to reach the products (P). It should be mentioned that, for the four considered decomposition reactions, any attempt to localize a stepwise mechanism involving HO^--promoted H^+ removal and N–Cl bond-breaking was unsuccessful.

Harmonic frequencies were calculated in order to confirm the nature of the stationary points, one imaginary frequency for TSs and zero for local minima. Zero-point energies and thermal corrections to enthalpies and free energies at 298.15 K have been taken into account. The unique imaginary frequency associated with the transition vector (TV) of the different TSs has been analyzed.[23] The intrinsic reaction coordinate has been traced from the TSs down to the two lower energy structures (RIC and PIC), in order to verify that each saddle point links the two putative minima.[24–26]

Among the different procedures to describe solute–solvent interactions at the quantum level, the use of discrete water molecules and continuum models have been selected. High-level *ab initio* electronic structure calculations including even a modest number of solvent molecules are prohibitive computationally. On the other hand, continuum models are very popular due to their combination of simplicity and efficiency, however they are unlikely to be adequate for the description of the reaction under study in water, as a cavity is built around the bare solute, and therefore short-range solvent–solute interactions are not explicitly considered. The model employed in this work consists of *N*-chloro,*N*-methylethanolamine and HO^-, which promotes the reaction, with one discrete water molecule interacting with the incoming HO^- and another molecule acting as H^+ donor to the nitrogen atom of the amine. This cluster showed a good behaviour when studying the Hofmann elimination;[20] it can describe adequately the solute–solvent interaction in the first solvation layer by stabilization of localized charges, but long-distance solvent stabilization is ignored. Some authors endorsed the suitability of a hybrid approach using a combination of explicit solvent molecules and continuum model for the calculation of the solvation thermodynamic properties of ions, in particular HO^-.[27–30] Thus, a hybrid cluster-continuum model was considered. Single-point calculations were performed over the optimized microsolvated structures, using the polarized continuum model (PCM)[31] to estimate the Gibbs free energy of solvation, allowing a better description of the process in bulk water.[32]

It is important to remark that this kind of computational model must be used with caution. We do not claim that the inclusion of two discrete water molecules plus a continuum represented by a dielectric constant are enough for rigorously modelling the aqueous solvent, but apparently the inclusion of the continuum model and two water molecules produces a reasonable picture of the processes under study both in terms of structure and energy.

Evolution of relevant bonds along each reaction pathway was calculated using the natural population analysis of Weinhold *et al.*[21,33–35] In order to analyse the synchronicity of the four pathways, the S_y parameter proposed by Moyano *et al* has been used.[36,37]

Results

Energy and reactivity

Fig. 1 shows the free energy profiles for the four decomposition processes under study. Fig. 1(left) collects microsolvated data, *i.e.*, including two discrete water molecules, and Fig. 1(right) shows the results obtained with the hybrid microsolvated-continuum model. Three stationary points have been characterized on the PES: the RIC, the TS, and the corresponding PIC; for comparison purposes the reactants were taken as reference. Although the four pathways correspond to different chemical processes, and thus the reaction centres and products are not the same (Scheme 2), the free energy

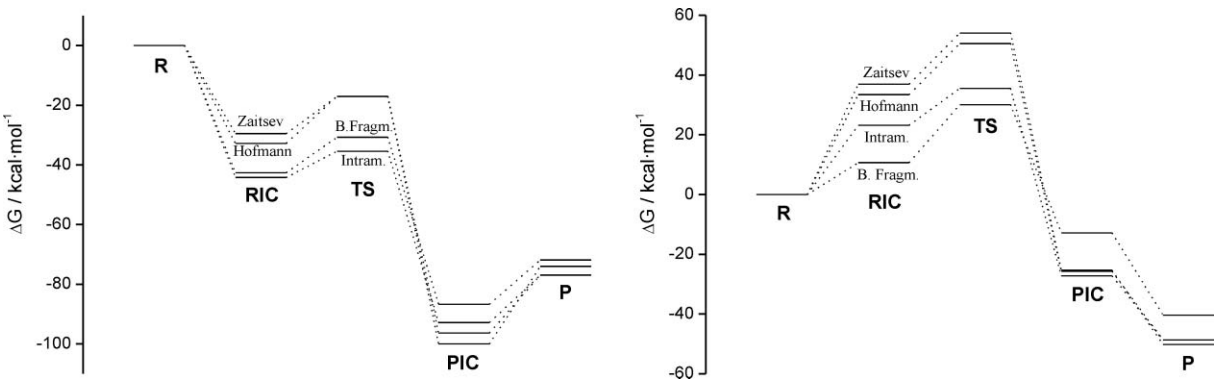

Fig. 1 Gibbs free energy profiles for the four pathways found for the HO^--promoted decomposition of *N*-chloro,*N*-methylethanolamine at the MP2=full/6-31++G(d,p) computational level. Reactants (R) were taken as reference. Data obtained with microsolvated (left) and microsolvated plus continuum (right) models.

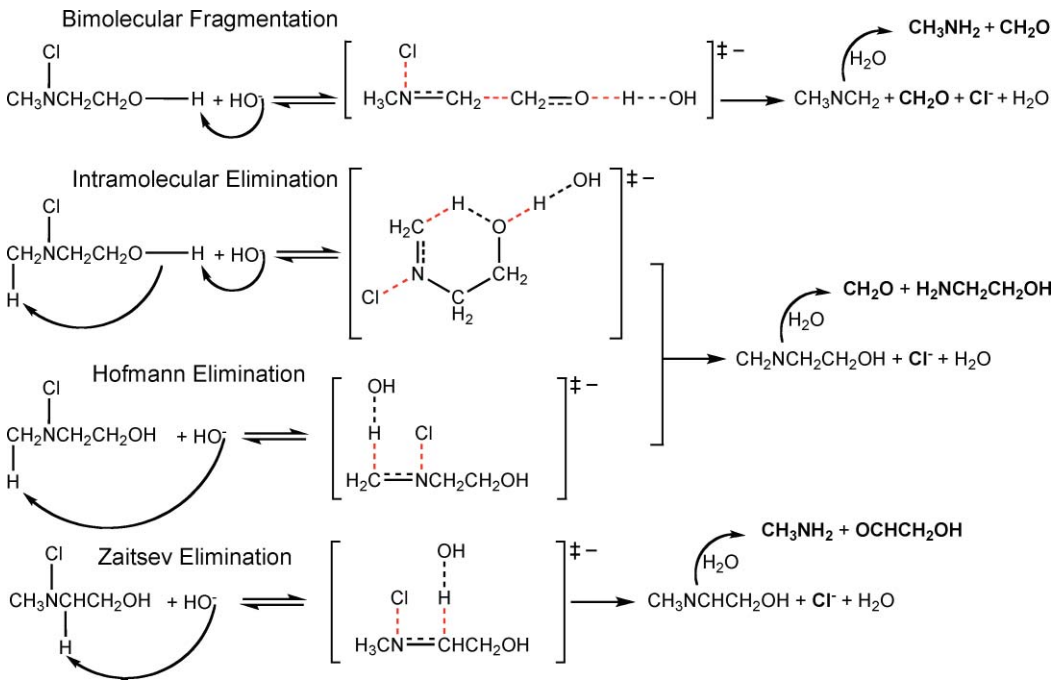

Scheme 2 The four parallel pathways involved in the rate-determining step of the HO^--promoted decomposition of *N*-chloro,*N*-methylethanolamine. Bonds being broken (in red) and formed (in black) are shown as dashed lines. End products through each pathway are shown in bold. Notice that the products of Hofmann and intramolecular eliminations are the same, and thus these two pathways are indistinguishable by product analysis.

profiles obtained are similar. Reaction pathways produced by the microsolvated model present an inverted energy profile in all cases – Fig. 1(left) – while the deep effect of solvation is evident in Fig. 1(right).

Despite the fact that RIC and/or PIC do not represent true minima on the PES when the continuum model is used to describe reactions in solution, we have retained them in the computational study with the hybrid cluster-continuum model. A physical meaning has been traditionally assigned to RIC and PIC in solution. Many bimolecular steps in solution can be described similarly to the mechanism of proton transfer first proposed by Eigen;[38] such bimolecular processes involve the passage through three well defined stages: 1) diffusion together of reactants to give an encounter complex (here named RIC); 2) electron and/or molecular rearrangement, *i.e.*, the chemical change associated to the bond-breaking/bond-forming processes involved in TSs; and, if appropriate, 3) dissociation of the product's encounter complex (here named PIC) into separate products.[38] This conceptual scheme can be also translated quantitatively into kinetics by using Marcus' theory:[38]

$$\Delta G^{\circ\ddagger} = w^{r} + \Delta G_0^{\circ\ddagger}\left(1 + \frac{\Delta G_e^{\circ}}{4\Delta G_0^{\circ}}\right)$$

where the work term w^r represents the standard molar free-energy involved in bringing reactants together in the right configuration for the chemical event to take place, *i.e.* $\Delta G^{\circ}(\mathrm{R} \rightarrow \mathrm{RIC})$. The meaning of other terms is described elsewhere.[38]

Calculated thermodynamic parameters are reported in Table 1. In both models, reactions can be described as three sharply separable parts: (a) the formation of RIC from reactants corresponds to an activationless process in the microsolvated model, while the approach of the incoming HO^- and *N*-chloro,*N*-methylethanolamine to form the RIC requires a minimum of 20 kcal mol^{-1} in the hybrid microsolvated-continuum model. In the microsolvated model, energy reduction comes from the stabilization of ions (HO^-) by hydrogen bonding with the amine and/or water molecules, whereas in the hybrid discrete-continuum model, bulk solvation stabilizes more the charge present in reactants than the more diffused charge in RIC; (b) bond-breaking/bond-forming processes corresponding to the formation of the TSs of the four parallel pathways under study. The N–Cl bond is always broken, a C–N single bond is transformed into a C=N double bond (imine), and the corresponding H atom is transferred from *N*-chloro,*N*-methylethanolamine to the incoming HO^-. Further reorganization is also carried out according to each molecular process (Scheme 2); (c) formation of energetically more stable PIC and products (P). The position of P with respect to PIC also depends on the presence of the continuum model.

In the microsolvated model – Fig. 1(left) – the Gibbs free energy of activation corresponds to the intrinsic free energy barrier going from RIC to TS, labelled $\Delta G^{\circ}_{\mathrm{int}}$. According to this model, the intramolecular elimination pathway exhibits the lowest free energy of activation (Table 1). The obtained order of reactivity is: intramolecular elimination > bimolecular fragmentation > Zaitsev elimination > Hofmann elimination.

Although the structural parameters were not modified, addition of PCM bulk solvent, *i.e.*, hybrid cluster-continuum model, led to an effective change in all free energy reaction profiles, as reported in Table 1 and shown in Fig. 1(right). The formation of structures with RIC geometries is an activated process, while the corresponding TSs are now located above the reference R. In the initial step, partial desolvation of the reagents, mainly HO^-, gives rise to a free energy barrier in contrast to the microsolvated model. This result is consistent with those obtained for other reactions involving HO^- attack calculated by different computational methods, such as PCM-B3LYP,[39] Monte Carlo[40] or QM/MM molecular dynamics.[41] In all cases, $\Delta G^{\circ}_{\mathrm{int}}$ increases when PCM solvation is incorporated (Table 1). The lowest free energy intrinsic barrier of the four processes is again obtained for the intramolecular elimination. Similar activation Gibbs energy values were calculated for the Hofmann and Zaitsev eliminations, while bimolecular fragmentation presents the largest value of the barrier height.

A detailed analysis of solvation in going from RIC to TS, in the hybrid cluster-continuum model, shows that the main and energetically favourable contribution comes from the electrostatic term (Table 2), while the average contribution of the non-electrostatic term is positive and amounts to about 0.5 kcal mol^{-1}. The RIC of bimolecular fragmentation shows the most negative solvation energy, whereas similar values are found for the rest of RICs. The same pattern applies for TSs, but stabilization due to solvation is lower, and consequently destabilization is obtained in going from RIC to TS, this effect being stronger in the case of bimolecular fragmentation. Although there is no unique way to separate electrostatic and non-electrostatic contributions to the free energy of solvation,[42] results will not differ using other partition schemes.

Table 1 Thermodynamic parameters, ΔH, $T\Delta S$ and ΔG (in kcal mol^{-1}) for the four parallel pathways of HO^--promoted decomposition of *N*-chloro,*N*-methylethanolamine obtained at the MP2=full/6-31++G(d,p) level (T = 298.15 K). Reactants (R) were taken as reference (total energy of R in kcal mol^{-1}: $H = -587266.68$, $TS = 63.88$, $G = -587330.57$, $G_{\mathrm{solvation}} = -117.16$). ΔG_{int} values refer to intrinsic activation barrier ($\Delta G_{\mathrm{int}} = \Delta G_{\mathrm{TS}} - \Delta G_{\mathrm{RIC}}$). Values of Gibbs free energy obtained with PCM continuum model are in italics. w^r parameter from Marcus' equation corresponds to $\Delta G(\mathrm{R} \rightarrow \mathrm{RIC})$ (ref. 38). Values between parentheses calculated at the DFT/B3LYP/6-31++G(d,p) level (ref. 14 and 20). $\Delta G^{\ddagger}_{\mathrm{exp}}$ refers to the experimental activation barriers (ref. 14)[a]

	RIC			TS					PIC			P		
	ΔH°	$T\Delta S^{\circ}$	ΔG° w^r	ΔH°	$T\Delta S^{\circ}$	ΔG°	ΔG_{int}	$\Delta G^{\ddagger}_{\mathrm{exp}}$	ΔH°	$T\Delta S^{\circ}$	ΔG°	ΔH°	$T\Delta S^{\circ}$	ΔG°
Hofmann elim.	–59	–26	–33, *34*	–45	–28	–17, *51*	16, *17* (7.5, *0.78*)	*24*	–120	–23	–96, *–26*	–67	9.6	–77, *–49*
Zaitsev elim.	–56	–26	–29, *37*	–43	–26	–17, *54*	12, *17*	*23*	–124	–24	–100, *–25*	–63	11	–74, *–50*
Bimol. fragm.	–68	–25	–43, *11*	–53	–22	–31, *30*	12, *19*(6.5, *3.6*)	*19*	–105	–18	–87, *–13*	–50	22	–72, *–40*
Intramol. elim.	–69	–25	–44, *23*	–60	–24	–35, *35*	8.8, *12*	*20*	–113	–20	–93, *–27*	–67	9.6	–77, *–49*

[a] Values rounded to show two significant figures.

Table 2 Contribution of the electrostatic and non-electrostatic terms to the solvation energy in the four parallel base-promoted decomposition pathways. All values in kcal mol^{-1} [a]

	Hofmann elimination	Zaitsev elimination	Bimolecular fragmentation	Intramolecular elimination
RIC				
Electrostatic term	–60	–60	–74	–59
Non-electrostatic term	7.2	7.8	7.9	7.5
TS				
Electrostatic term	–58	–55	–66	–55
Non-electrostatic term	6.7	7.5	7.3	7.2
RIC → TS	1.8	5.1	8.2	3.9
$\Delta G_{electrostatic}$	–0.52	–0.37	–0.66	–0.34
$\Delta G_{non\text{-}electrostatic}$	1.3	4.8	7.5	3.5
$\Delta G_{solvation}$	–60	–60	–74	–59

[a] Values rounded to show two significant figures.

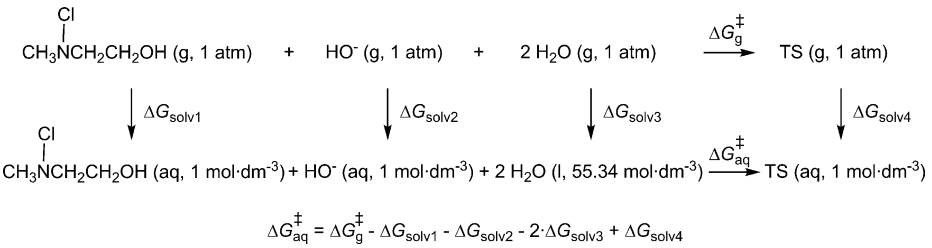

Scheme 3 Thermochemical cycle used to estimate the activation Gibbs free energy in aqueous solution.

Values for absolute activation Gibbs free energies, ΔG°(R → TS), with the cluster-continuum hybrid model (Table 1) have been calculated by using the thermochemical cycle shown in Scheme 3. The corresponding values have been corrected in order to use consistent standard states.[43]

Geometry

Geometries of TSs, connecting RIC and PIC, for each model system are shown in Fig. 2, and representative structural parameters of calculated stationary points are collected in the ESI†.

TSs for Hofmann, Zaitsev, and intramolecular elimination processes exhibit cyclic arrangements (Fig. 2), but only in the latter are any bonds of the ring broken/formed (see Scheme 2). These cyclic assemblies contribute to stabilize the TSs, distributing more uniformly atomic charges; in fact their dipole moments are lower than that of bimolecular fragmentation (see ESI). In the intramolecular elimination a six-membered ring is formed by the bent backbone of *N*-methylethanolamine; both edges are linked by the hydrogen atom that is being transferred from methyl carbon atom (C_1) to the alcoholic oxygen (Fig. 2). Non reaction-active 7-membered rings are obtained in the TSs of the intermolecular eliminations, Hofmann and Zaitsev; such cyclic arrangements involve the ethanolamine fragment of the *N*-chloro compound and one of the discrete water molecules used to model specific solute–solvent interactions (Fig. 2).

Those 7-membered cyclic assemblies present two hydrogen bonds: the water molecule acts both as H^+ donor/acceptor to/from the nitrogen/oxygen atom of *N*-chloro,*N*-methylethanolamine, respectively. A linear arrangement is obtained in the TS of the bimolecular fragmentation (Fig. 2).

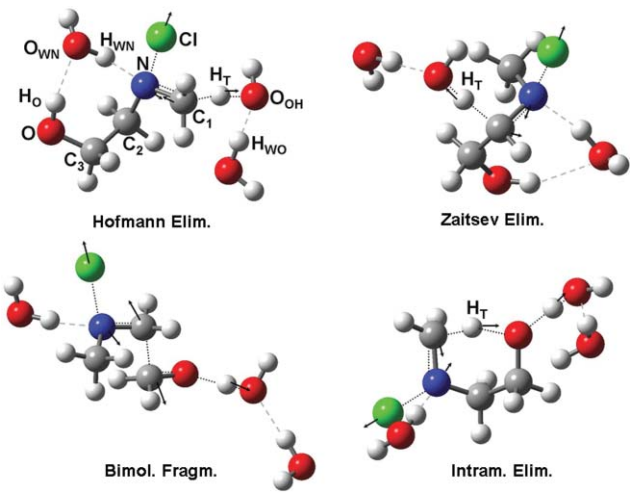

Fig. 2 Optimized transition structures for the four decomposition pathways obtained at the MP2=full/6-31++G(d,p) level. Breaking/forming bonds are displayed as dotted lines, while hydrogen bonds are represented by dashed lines. Vibrational mode components in mass-weighted coordinates are also included. Atom numbering used through the paper is indicated: H_T is the proton transferred from a carbon atom, either C_1 or C_2, in the elimination reactions; H_O labels the proton initially bound to the alcohol group; two explicit hydrogen bonded water molecules are taken into account, one acting as H^+ donor to the O atom of incoming HO^- and the other to the N atom; these are labelled as WO and WN, respectively.

Transition vectors (TV) and bonds evolution

The transition vectors for the different TSs are represented in Fig. 2. The components of TV for the different pathways are clearly associated with the bond-forming/bond-breaking

processes. Thus, in the four pathways TVs are coupled with a proton transfer (H_T or H_O) to the oxygen atom (O_{OH}) of the incoming HO^-, formation of a C=N double bond (imine) and Cl^- acting as nucleofuge. In all cases the discrete water molecules also participate in the TV.

Evolution of relevant bonds along the reaction coordinate (see ESI) confirms the behaviour revealed by TVs analysis. Four different bonds are concertedly formed/broken in the intermolecular Hofmann and Zaitsev eliminations, while six bonds are converted in the other two processes (Scheme 2). Again, the shared features of the four pathways are imine formation, N–Cl cleavage and proton transfer to the incoming HO^-, the latter being ahead of the other molecular processes. This indicates that HO^- approach and subsequent proton abstraction triggers the decomposition mechanism.

Atomic charges

Electron flow takes place along the reaction from the incoming HO^- to the leaving Cl^- (relevant Mulliken atomic charge values are collected in the ESI). The net atomic charge of the H atoms being transferred at the TSs increases from R to TS due to the enhancement of the polarity of the bonds being formed/broken. This value ranges from 0.30 to 0.56 a.u.. In addition, at the TSs the net negative charge displaced from the hydroxide moiety varies in the range 44–71% of the total charge transferred along the whole process, and the chlorine fragment holds a net negative charge between 0.23–0.48 a.u. depending on the pathway under consideration.

Discussion

It has been observed experimentally that the decomposition reaction of *N*-chloro,*N*-methylethanolamine in basic medium fulfils a second-order rate law, being first-order relative to both chloramine and base,[14] *i.e.*, in the present case:

$$r = k_{obs} \times [N\text{-chloro},N\text{-methylethanolamine}] \times [HO^-]$$

As stated above, the net reaction is more complex, the final products being Cl^-, an aldehyde, and an amine with at least one carbon less. Kinetic experiments are consistent with the Cl^- leaving as a nucleofuge, the imine formation and the proton cleavage taking place in the rate-limiting step,[2,13,14] which could be classified as an asynchronous concerted process.[14] Subsequent hydrolysis of the imine is much faster than its formation, *i.e.*, such hydrolysis has no influence on the observed rate of *N*-chloro,*N*-methylethanolamine decomposition.[2]

Previous density functional theory (DFT) calculations on the Hofmann rearrangement[20] allowed us to establish a suitable model to simulate the reaction in water, and therefore, it was employed again, this time at the *ab initio* MP2 =full/6-31++G(d,p) computational level. Transition vectors (Fig. 2) obtained for the four pathways taking place in the HO^--promoted decomposition of *N*-chloro,*N*-methylethanolamine, agree with each process being a bimolecular concerted step, which fits to overall second-order kinetics as well.

Description of those molecular processes is consistent with the proposed detailed reaction pathways coming from experimental studies.[2,14] Six bonds are involved along the breaking/forming processes of the intramolecular elimination and bimolecular fragmentation, while only four bonds are directly involved in the Hofmann and Zaitsev eliminations (Scheme 2 and ESI).[14]

At the TSs all H atoms being transferred to OH^- increase their positive charge between 0.14 and 0.37 a.u.; therefore, the reaction has a proton transfer character. The other H atom "in flight" in the intramolecular elimination (H_T) is also 0.16 a.u. more positive at TS; the process can also be considered as a proton transfer. All proton transfer processes take place along geometrical linear arrangements (bond angles >170°), except that of the 6-membered ring in the intramolecular elimination (155°). At the TSs the bond between H^+ and HO^- is more than 55% formed (ESI), except in the Zaitsev elimination, where this value is lower (34%). Bond evolution values indicate that proton transfer to HO^- triggers the rest of the molecular events (Scheme 2).

In the four pathways the corresponding imine is formed, and Cl^- acts as nucleofuge; additionally, formaldehyde works as electrofuge in the bimolecular fragmentation. Depending on the elementary step the N–Cl bond is broken between 7.1% and 37.5% at the TS. The increase of the Cl atom negative charge along the reaction coordinate is coupled with the decrease of the charge on the oxygen of the HO^- moiety; therefore, there is a synergetic charge flow generating an anion at the Cl-end (charges and bond evolution data are collected in the ESI).

The net charge on N atom does not vary, relative to reactants, in either the Hofmann or Zaitsev eliminations, whereas it is less negative in the other two pathways; this is consistent with the degree of N–Cl bond-breaking at the different TSs. The interaction of the discrete water molecule in the neighbourhood of the amino group is reflected in the more negative charge on the N atom both at RIC and PIC. Consequently, there is a polarization effect on this water molecule, which stays fairly constant for each pathway when moving from RIC to PIC. Similar behaviour is obtained for the discrete water molecule near HO^-; in this case the negative charge of the oxygen decreases on going from RIC to TS due to the partial conversion of hydroxide ion into a water molecule. Finally, charge on the C atom involved in the formation of C–N double bond, C_1 or C_2, acquires its most negative value at the TS.

The synchronicity values, S_y, as calculated from the bonds being formed or broken along the four reaction pathways, are collected in the ESI. $S_y = 1$ implies fully synchronous bond reorganization, while $S_y = 0$ characterizes a stepwise mechanism; thus the S_y values support our previous analysis, *i.e.*, all pathways are concerted but not fully synchronous, the order of synchronicity being: Zaitsev elimination < Hofmann elimination < intramolecular elimination < bimolecular fragmentation. The value obtained here for the bimolecular fragmentation is similar to that found with the DFT(B3LYP)/6-31++G(d,p) model.[14]

Synchronicity can also be calculated from empirical kinetics as $(1 - |\beta_H - |\beta_{lg}||)$,[14] where Brønsted's β_H gives an estimation of the O–H_O bond-breaking at the TS, and the Brønsted-like parameter β_{lg} measures the degree of N–Cl bond-breaking at the TS.[38] Brønsted's β_H values for the intramolecular elimination and bimolecular fragmentation pathways are 0.45 and 0.60 respectively.[14] These values are consistent with what was obtained here, the evolution of O–H_O bond-breaking at the TSs being calculated as 83.3% ($\beta_H = 0.833$) for the elimination, and 82.8% ($\beta_H = 0.828$) for the fragmentation. Experimental values have large uncertainties due to the curvature of the Brønsted plot, an observation already found

for analogous base-promoted processes.[44] On the other hand, values of β_{lg}, estimated from experimental reaction rates obtained for the process under study for the chlorinated and brominated species, are –0.2 and –0.35 for bimolecular fragmentation and intramolecular elimination, respectively, their uncertainty being unknown, as only two values were used to calculate β_{lg}.[14] Thus, empirical values for synchronicity are 0.60 for the fragmentation and 0.90 for the elimination. Keeping in mind the approximations underlying those values, the agreement with the theoretical ones is acceptable (see ESI). These results imply that the four pathways correspond with asynchronous concerted bimolecular processes.

Free energy activation barriers, and therefore kinetic constants, differ significantly from experimental data (Table 1). According to the microsolvated model, the intramolecular elimination is the preferred pathway, its activation free energy being the lowest of the four competitive processes, as experimentally predicted by the extremely slow rate measured for *N*-chloro,*N*-(*tert*-butyl)ethanolamine decomposition reaction.[13] On the other hand, the experimental study with *N*-chloro,*N*-methylethanolamine and HO^- pointed to the bimolecular fragmentation as the main decomposition pathway (67%), while the intramolecular pathway accounted for the remaining 33% of the reaction.[14] This partition into pathways was based on product analysis.

Addition of PCM to the microsolvated model increases activation barriers for all pathways in the present study, whereas the opposite was found for Hofmann elimination and bimolecular fragmentation at the less-demanding DFT-based B3LYP/6-31++G(d,p) level (see Table 1).[14,20] Values for ΔH°, $T\Delta S^\circ$ and ΔG° are more negative when MP2 instead of DFT is used; on the other hand, energy barriers increase with the former when single-point PCM calculations are included. This indicates that both computational methods, using the same basis set, differ on the free energy assignment of continuum-solvated models of RICs and TSs, thus yielding opposite solvation effects on the ΔG°_{int} values. Activation free energy increases, since charge polarization – and therefore solvent stabilization – on the RIC is higher than in the TS (see Mulliken charges and dipolar moment in the ESI); thus, polar solvents like water stabilize the former more efficiently than the latter. When PCM solvation is considered, the reactivity pattern is different from that in the case of the microsolvated model; then the intramolecular elimination is still the fastest pathway, while the bimolecular fragmentation becomes the slowest one.

One could wonder which barrier really corresponds to the activation free energy, $\Delta G^\circ(\mathrm{RIC} \rightarrow \mathrm{TS})$ (*i.e.*, ΔG°_{int}) or $\Delta G^\circ(\mathrm{R} \rightarrow \mathrm{TS})$. In the absence of bulk solvation, there is no doubt that ΔG°_{int} is the energy barrier; whereas $\Delta G^\circ(\mathrm{R} \rightarrow \mathrm{TS})$ could be adequate for processes in solution when non-inverted free energy reaction profiles are found – see Fig. 1(right). This is caused by the partial desolvation of approaching reactants that is not sufficiently compensated by the additional interaction energies; in that case, RIC and PIC are not stationary structures. As stated before, geometries of PCM-solvated structures were not optimized, we just carried out single-point calculations including the continuum model. Attempts to obtain unconstrained optimized structures of some of the stationary points including PCM were unsuccessful, even with Gaussian03.

All activation free energy values mentioned above have been obtained as ΔG°_{int}. However, the picture changes when the energy barrier is calculated between R and TS, as depicted in Fig. 1(right). In this case the kinetically favoured process is the bimolecular fragmentation, as experimentally found,[14] followed by the sequence: intramolecular, Hofmann and Zaitsev eliminations.

Both microsolvated and microsolvated plus PCM models predict a high acceleration of the decomposition reaction, *i.e.*, lower activation free energies, when the alcohol group is directly involved in the reaction, which is consistent with the dramatic (360-fold) rate acceleration experimentally observed when alcoholamines instead of parent amines are studied.[14] Fully optimized electronic structure calculations at the relatively sophisticated MP2/6-31++G(d,p) level and with a hybrid-continuum model to describe solvation effects, often, like here, misjudge the absolute thermodynamic values even for simple reactions; however, the relative acceleration caused by the alcohol group is properly predicted.

The title decomposition reaction has only been described up to the point where the chloride anion departs and the imine forms, while much less attention was paid to the subsequent hydrolysis of imines even though the partition on different pathways is based on product analysis from such imine hydrolysis.[14] Imine hydrolysis has been considered to take place as suggested by Jencks and coworkers,[45,46] and repeatedly verified afterwards. This process involves an uncatalyzed pathway, and is also subject to general base catalysis;[47] thus, under the experimental conditions, the process would be accelerated. This second process seems to be faster, so that the previously described processes represent the rate-limiting step in all cases. Although decomposition reaction rates, and therefore observed kinetic rate constants, are not affected by the subsequent faster imine hydrolysis, this second step should be carefully taken into account since partition into pathways is performed on the basis of product analysis.[14] As shown in Scheme 2, imines produced through different pathways are not identical; the -OH group of the parent ethanolamine remains in imines coming from the three elimination processes, whereas it is absent in the imine formed in the bimolecular fragmentation pathway. Furthermore, when multiple functionality is present elsewhere in the molecule, imines may suffer from other side reactions[48] like tautomerization; thus, unexpected products are feasible, which could lead one to misinterpret the relative contribution of the four pathways involved in the rate-determining step of the base-promoted decomposition of aliphatic secondary *N*-chloroethanolamines. Work is in progress to explore this issue.

Conclusions

In this work, the rate-limiting step of the HO^--induced decomposition of *N*-chloro,*N*-methylethanolamine in water has been investigated using the MP2/6-31++G(d,p) method. To give an appropriate picture of this process, a microsolvated model (in which two explicit water molecules simulate the specific solvent effects) and a hybrid cluster-continuum model (by applying PCM on the previous results, to account for the bulk effect of solvent) have been explored. Our calculations showed that the reaction takes place *via* four different competitive pathways (bimolecular fragmentation, and Hofmann, Zaitsev and intramolecular eliminations). The results indicated that all pathways can be considered as bimolecular asynchronous concerted processes; proton transfer to HO^- is more advanced than all other molecular events, whereas imine formation is delayed. TSs of Hofmann, Zaitsev,

and intramolecular eliminations have cyclic structures, only the latter being reactive. Hofmann and Zaitsev mechanisms involve a water molecule that acts both as H^+ donor/acceptor to/from the nitrogen/oxygen atom of *N*-chloro,*N*-methylethanolamine, respectively.

Computational studies agree with experimental findings in the global description of the processes, even accounting for the dramatic acceleration of the decomposition process due to the addition of an alcoholic group on C_β to the amino group of *N*-chloro,*N*-methylethylamine.

According to the microsolvated model, intramolecular elimination is the most favourable decomposition pathway. On the other hand, our results indicate that the continuum increases all reaction barriers, lowering the computed rate constants, and when considering the free energy of activation from reactants, ΔG ($R \rightarrow TS$), bimolecular fragmentation is the preferred decomposition pathway, as found empirically in the reaction between HO^- and *N*-chloro,*N*-methylethanolamine.[14] To the best of our knowledge, this paper is the first comprehensive computational study on the molecular mechanism for the reaction between *N*-chloro aliphatic secondary ethanolamines and bases.

Acknowledgements

D.R.R. thanks the grants of the former Spanish *Ministerio de Educación*, *Cultura y Deporte* (F.P.U. program, 2000–2003), and of the Universidade da Coruña (2004–2005). This work was supported by research funds provided by the *Ministerio de Educación y Cultura* of the Spanish Government by DGICYT projects: BQU2003-04168-C03-03 (J.A. and R.C.) and CTQ2004-00534/BQU (D.R.R., M.C.L., M.V.G., and J.A.S.); by the *Generalitat Valenciana*—project GV06/016—(J.A. and R.C.), and by the *Xunta de Galicia*—project PGIDIT05PXIC10306PN—(D.R.R., M.C.L., M.V.G., and J.A.S.). We are indebted to the *Centro de Supercomputación de Galicia* (CESGA) for computer capabilities.

References

1 H. Maskill, *The Investigation of Organic Reactions and their Mechanisms*, Blackwell Publishing, Oxford, 2006.
2 X. L. Armesto, M. Canle, L., M. V. García and J. A. Santaballa, *Chem. Soc. Rev.*, 1998, **27**, 453.
3 S. Miller, *Environ. Sci. Technol.*, 1993, **27**, 2292.
4 M. T. Do, N. J. Birkett, K. C. Johnson, D. Krewski, P. Villeneuve and Canadian Cancer Registries Epidemiology Research Group, *Environ. Health Perspect.*, 2005, **113**, 418.
5 T. Oppenländer, *Photochemical Purification of Water and Air: Advanced Oxidation Processes (AOPs): Principles, Reaction Mechanisms, Reactor Concepts*, Wiley-VCH, Weinheim, 2003.
6 S. J. Klebanoff, *J. Bacteriol.*, 1968, **95**, 2131.
7 I. U. Schraufstätter, K. Browne, A. Harris, P. A. Hyslop, J. H. Jackson, O. Quehenberger and C. G. Cochrane, *J. Clin. Invest.*, 1990, **85**, 554.
8 E. L. Thomas, M. B. Grisham and M. M. Jefferson, *J. Clin. Invest.*, 1983, **72**, 441.
9 S. J. Klebanoff, in *Inflammation: basic principles and clinical correlates*, eds. J. I. Gallin and R. Snyderman, Lippincott Williams & Wilkins, Philadelphia, 1999, p. 721.
10 C. S. Foote, T. E. Goyne and R. I. Lehrer, *Nature*, 1983, **301**, 715.
11 D. R. Ramos, M. V. García, M. Canle, L., J. A. Santaballa, P. G. Furtmüller and C. Obinger, *J. Inorg. Biochem.*, 2008, **102**, 1300.
12 D. R. Ramos, M. V. García, M. Canle, L., J. A. Santaballa, P. G. Furtmüller and C. Obinger, *Arch. Biochem. Biophys.*, 2007, **466**, 221.
13 X. L. Armesto, M. Canle, L, P. Carretero, M. V. García and J. A. Santaballa, *Tetrahedron*, 1997, **53**, 2565.
14 J. Andrés, X. L. Armesto, M. Canle, L, M. V. García, D. R. Ramos and J. A. Santaballa, *Org. Biomol. Chem.*, 2003, **1**, 4323.
15 J. Xiao, C. W. Li and M. H. Li, *Chem. Eng. Sci.*, 2000, **55**, 161.
16 D. L. Nelson and M. M. Cox, *Lehninger Principles of Biochemistry*, W. H. Freeman, New York, 2008.
17 S. M. Austin and T. G. Waddell, *Orig. Life Evol. Biosph.*, 1999, **29**, 287.
18 K. Yamamoto, Y. Takahashi, T. Mano, Y. Sakata, N. Nishikawa, J. Yoshida, Y. Oishi, M. Hori, T. Miwa, S. Inoue and T. Masuyama, *Eur. Heart J.*, 2004, **25**, 1221.
19 C. Liao and R. A. Nicholson, *Eur. J. Pharmacol.*, 2007, **566**, 103.
20 D. R. Ramos, R. Castillo, M. Canle, L., M. V. García, J. Andrés and J. A. Santaballa, *Chem. Phys. Lett.*, 2006, **429**, 425.
21 M. J. Frisch, G. W. Trucks, H. B. Schlegel, G. E. Scuseria, M. A. Robb, J. R. Cheeseman, V. G. Zakrzewski, J. A. Montgomery, R. E. Stratmann, J. C. Burant, S. Dapprich, J. M. Millam, A. D. Daniels, K. N. Kudin, M. C. Strain, O. Farkas, J. Tomasi, V. Barone, M. Cossi, R. Cammi, B. Mennucci, C. Pomelli, C. Adamo, S. Clifford, J. Ochterski, G. A. Petersson, P. Y. Ayala, Q. Cui, K. Morokuma, D. K. Malick, A. D. Rabuck, K. Raghavachari, J. B. Foresman, J. Cioslowski, J. V. Ortiz, B. B. Stefanov, G. Liu, A. Liashenko, P. Piskorz, I. Komaromi, R. Gomperts, R. L. Martin, D. J. Fox, T. Keith, M. A. Al-Laham, C. Y. Peng, A. Nanayakkara, C. Gonzalez, M. Challacombe, P. M. W. Gill, B. G. Johnson, W. Chen, M. W. Wong, J. L. Andres, M. Head-Gordon, E. S. Replogle and J. A. Pople, *Revision A.7*, Gaussian, Inc., Pittsburgh PA, 1998.
22 C. Møller and M. S. Plesset, *Phys. Rev.*, 1934, **46**, 618.
23 J. W. McIver, *Acc. Chem. Res.*, 1974, **7**, 72.
24 K. Fukui, *J. Phys. Chem.*, 1970, **74**, 4161.
25 C. Gonzalez and H. B. Schlegel, *J. Phys. Chem.*, 1990, **94**, 5523.
26 C. Gonzalez and H. B. Schlegel, *J. Chem. Phys.*, 1991, **95**, 5853.
27 C. Cappelli, B. Mennucci, C. O. Silva and J. Tomasi, *J. Chem. Phys.*, 2000, **112**, 5382.
28 A. R. Grimm, G. B. Bacskay and A. D. Haymet, *Mol. Phys.*, 1995, **86**, 369.
29 I. Tuñón, D. Rinaldi, M. F. Ruiz-López and J. L. Rivail, *J. Phys. Chem.*, 1995, **99**, 3798.
30 C. G. Zhan and D. A. Dixon, *J. Phys. Chem. A*, 2002, **106**, 9737.
31 J. Tomasi and M. Persico, *Chem. Rev.*, 1994, **94**, 2027.
32 J. R. Pliego, Jr. and J. M. Riveros, *J. Phys. Chem. A*, 2001, **105**, 7241.
33 J. E. Carpenter and F. Weinhold, *Theochem-J. Mol. Struct.*, 1988, **169**, 41.
34 E. D. Glendening, A. E. Reed, J. E. Carpenter and F. Weinhold, NBO Version 3.1.
35 A. E. Reed, L. A. Curtiss and F. Weinhold, *Chem. Rev.*, 1988, **88**, 899.
36 K. B. Wiberg, *Tetrahedron*, 1968, **24**, 1083.
37 A. Moyano, M. A. Pericas and E. Valenti, *J. Org. Chem.*, 1989, **54**, 573.
38 H. Maskill, *The Physical Basis of Organic Chemistry*, Oxford University Press, Oxford, 1986.
39 J. Kóňa, W. M. F. Fabian and P. Zahradník, *J. Chem. Soc. Perkin Trans. 2*, 2001, 422.
40 J. D. Madura and W. L. Jorgensen, *J. Am. Chem. Soc.*, 1986, **108**, 2517.
41 T. Hori, H. Takahashi and T. Nitta, *J. Comput. Chem.*, 2003, **24**, 209.
42 A. V. Marenich, C. J. Cramer and D. G. Truhlar, *J. Chem. Theory Comput.*, 2008, **4**, 877.
43 C. J. Cramer, *Essentials of Computational Chemistry. Theories and models*, John Wiley & Sons, Ltd, Chichester, 2004.
44 X. L. Armesto, M. Canle, L., M. V. García, M. Losada, P. Rodríguez and J. A. Santaballa, *Tetrahedron*, 1994, **50**, 2265.
45 W. P. Jencks, *J. Am. Chem. Soc.*, 1959, **81**, 475.
46 B. M. Anderson and W. P. Jencks, *J. Am. Chem. Soc.*, 1960, **82**, 1773.
47 E. H. Cordes and W. P. Jencks, *J. Am. Chem. Soc.*, 1963, **85**, 2843.
48 Z. H. Huang, D. C. Wan and J. L. Huang, *Chem. Lett.*, 2001, **30**, 708.

